

# Controlling mode orientations and frequencies in levitated cavity optomechanics

A. Pontin, H. Fu, J. Iacoponi, P.F. Barker and T.S. Monteiro<sup>1</sup>

<sup>1</sup>Department of Physics and Astronomy, University College London, Gower Street, WC1E 6BT London, United Kingdom.

Cavity optomechanics offers quantum cooling, quantum control and measurement of small mechanical oscillators. However the optical backactions that underpin quantum control can significantly disturb the oscillator modes: mechanical frequencies are shifted by the optical spring effect and light-matter hybridisation in strong coupling regimes; mechanical modes hybridise with each other via the cavity mode. This is even more pertinent in the field of levitated optomechanics, where optical trapping fully determines the mechanical modes and their frequencies. Here, using the coherent-scattering (CS) set-up that allowed quantum ground state cooling of a levitated nanoparticle, we show that - when trapping away from a node of the cavity standing wave- the CS field opposes optical spring shifts and mechanical mode hybridisation. At an optimal cancellation point, independent of most experimental parameters, we demonstrate experimentally that it is possible to strongly cavity cool and control the *unperturbed* modes. Suppression of the cavity-induced mode hybridisation in the  $x - y$  plane is quantified by measuring the  $S_{xy}(\omega)$  correlation spectra which are seen to always be anti-correlated except at the cancellation point where they become uncorrelated. The findings have implications for directional force sensing using CS set-ups.

There is currently intense interest in optical cooling of levitated nanoparticles both with cavities as well as active feedback methods [1]. Cooling with using optical cavities was proposed well over a decade ago, [2–6] but only in 2020 was ground state cooling achieved [7]: initial experimental efforts were plagued by technical difficulties of stable trapping in high vacuum [8, 9]. Several set-ups were investigated for cavity cooling including tweezer-cavity traps [2, 10], electro-optical traps [11, 12], and trapping in the near field of a photonic crystal [13]. Quantum cooling was also previously achieved with feedback cooling and quantum control [14, 15], but here we focus on levitated cavity optomechanical systems.

Recently, a 3D coherent scattering (CS) setup was introduced to levitated cavity optomechanics [16, 17] using methods adapted from atomic physics [18–22]. In contrast to experiments that consider dispersive coupling, here the cavity is driven solely by the dipole radiation of the optically trapped silica particle. The nanoparticle is trapped at the tight focus of the optical tweezer along the  $z$  axis and the tweezer laser polarisation angle and waist sets the orientation and frequencies  $\omega_x^{(0)}, \omega_y^{(0)}$  of the mechanical motion in the  $x - y$  plane. The CS set-up yielded unprecedentedly high optomechanical coupling rates  $g_x, g_y$ , which subsequently enabled ground-state cooling of the motion along the cavity axis and thus opened the door to quantum levitated optomechanics [7].

In [23, 24] it was shown analytically that  $x - y$  hybridisation resulted from both cavity mediated, back action terms and a direct coupling of the form  $g_{xy}\hat{x}\hat{y}$ . In effect the hybridisation was shown to yield a rotation of the normal modes in the  $x - y$  plane as well as hybridisation with optical modes, especially in strong-coupling regimes. The interesting case of  $g_x \simeq g_y$  which is obtained experimentally for tweezer polarisation angle  $\theta = \pi/4$ , in the strong-coupling regime produces a rotation angle of  $\pi/4$  and leads to the formation of dark and bright modes [24, 25].

The set-up is illustrated in **Fig.1** : we investigate the

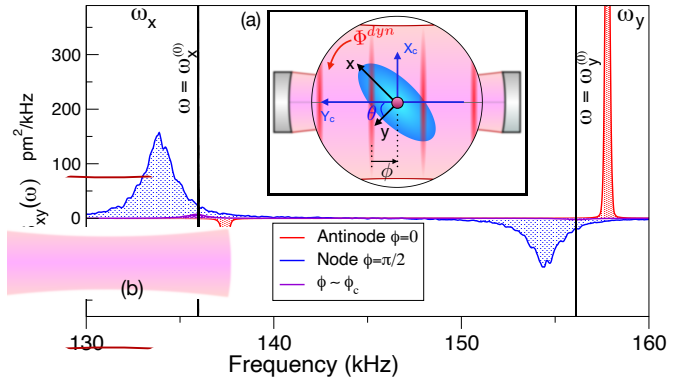


FIG. 1. (a) Inset illustrates a nanoparticle trapped by an optical tweezer, with  $x - y$  mechanical modes. However, the presence of a surrounding cavity, aimed at quantum cooling, hybridises the modes and shifts their unperturbed frequencies  $\omega_{x,y}^{(0)}$ . The experimental tweezer polarisation sets an initial angle  $\theta$  between the  $x - y$  modes and cavity axis. Then, the optomechanical cavity hybridisation dynamics adds an effective mode rotation  $\Phi^{dyn}$ , where  $\Phi^{dyn} \simeq \theta$  leads to formation of dark/bright modes. However, away from optical nodes, the CS field opposes this effect. (b) We investigate mode orientation by measuring cross-correlation spectra  $S_{xy}(\omega)$  for  $\theta \simeq \pi/4$  as the trapping position is swept from node ( $\phi = \pi/2$ ) to antinode ( $\phi = 0$ ) of the cavity standing wave. The  $x - y$  motions are always anticorrelated (peaks of opposite sign), but  $S_{xy}$  flips sign at  $\phi = \phi_c$ . for this value, the CS field cancels  $\Phi^{dyn}$ : the mechanical modes are locked at their unperturbed orientations *and* unperturbed frequencies for arbitrary power and for detuning  $\Delta \gg \omega_{x,y}$ , but can still be strongly cooled. The results have implications for directional force sensing and, in strong coupling regimes, the suppression of dark/bright modes.

dynamical behavior of modes in the  $x - y$  plane experimentally. We show that the dynamical optical back-action contribution  $\Phi^{dyn}$  is, away from the node, opposed by a rotation caused by the direct couplings  $g_{xy}$  of the

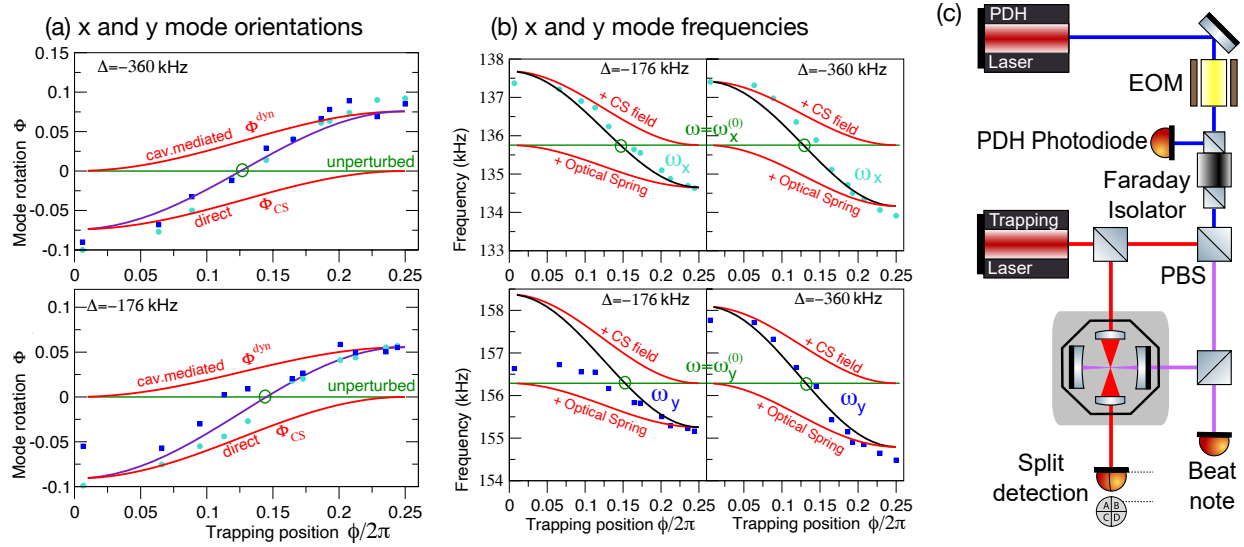


FIG. 2. (a) Measured orientation of modes in  $x - y$  plane. The mode rotation angle is  $\Phi(\phi)$ : it combines  $\Phi^{dyn}$ , a (positive sign) contribution from optomechanical backaction, thus an  $x - y$  coupling mediated by the optical mode fluctuations, and  $\Phi^{CS}$ , a (negative sign) contribution from the static CS field.  $\Phi^{dyn}$  is dominant at the node ( $\phi = \pi/2$ ) while  $\Phi^{CS}$  dominates at the antinode ( $\phi = 0$ ). Where they cancel (green circle,  $\phi = \phi_c$ ) the rotation is zero. The mode orientation is obtained from the measured correlation spectra,  $S_{xy}(\omega)$ , as shown in Fig.3 below: squares (blue) correspond to the  $y$  peak, circles (cyan) to the  $x$  peak. (b) Shows that the frequency behavior mirrors the mode rotation behavior: the optomechanical optical spring effect always softens the mechanical frequencies for red detuning. The CS field in contrast, stiffens the frequencies. At  $\phi \simeq \phi_c$  the two contributions cancel, leaving only the unperturbed mechanical frequency set by the tweezer trap. Red lines denote analytical optomechanical contributions, calculated from linearised equations of motion. Violet line shows their combined effect. (c) Experimental set-up, described in the text, along with experimental parameters.

CS set-up. In addition, we show here that the experimental mechanical frequency shifts directly mirrors this behaviour. At the node a dynamical term provides the optical spring softening. Away from the node the coherent scattering potential stiffens the mechanical frequency. The two effects cancel at the same point as the cancellation of the hybridisation. At this point the mechanical  $x, y$  frequencies both return to their unperturbed values and the modes are locked to their unperturbed orientation, for arbitrary experimental parameters. At the cancellation points, there is still strong optomechanical cavity cooling. However, this is at the cost of trapping away from the node, where the cavity photon occupancies are much higher ( $\sim 50$  times larger) than at the node [16]. We show that as the detuning tends to resonance, the cancellation point moves closer to the node so this disadvantage can be partially mitigated.

*Experimental set-up* A schematic overview of the experiment is shown in **Fig.2(c)**. We use two Nd:YAG lasers at a wavelength  $\lambda = 1064$  nm a weak field from the first is used to implement a Pound-Drever-Hall (PDH) scheme to lock it to a high finesse Fabry-Perot cavity. The second laser illuminates an optical tweezer (TW) composed of a single aspheric lens of nominal numerical aperture  $NA = 0.77$  and a symmetric condenser lens. The tweezer assembly is monolithic, is mounted on a 3-axes translational stage and includes an aspheric collection lens of  $NA = 0.3$ , oriented at  $90^\circ$  from the propagation

direction, which is exploited for imaging purposes. The TW trapping region is positioned at the center of the optical cavity which has a length  $L_{cav} = 12.23 \pm 0.02$  mm, a finesse  $\mathcal{F} \simeq 31000$  (linewidth  $\kappa/2\pi = 396 \pm 2$  kHz, input rate  $\kappa_{in} = 162 \pm 2$  kHz) and a waist of  $61 \mu\text{m}$ . The two lasers are phase offset locked by monitoring their beat note and their frequency separation is set to one free spectral range ( $\text{FSR} = c/2L_{cav} = 12.26 \pm 0.02$  GHz). The PDH beam is locked at resonance and the detuning of the trapping beam can be finely controlled. Importantly, the PDH beam is orthogonally polarized with respect to the TW beam and interacts with the particle only dispersively. This, in combination with the low power makes the role of the PDH beam in the dynamics negligible. The motion of the particle in the TW polarization plane is monitored by distributing the TW light collected by the condenser lens to two balanced detectors. Each detector is balanced using D-shaped mirrors oriented parallel and perpendicular to the beam polarization. The two detectors can measure independently the  $x$  and  $y$  motion with a rejection ratio potentially exceeding  $-30$  dB, however, any imperfections in the orientations of the D-mirror can result in a small mixing of  $x$  and  $y$  in the detected signals.

*Physical model:* in a coherent scattering (CS) approach, the optical cavity is not externally driven but it is populated exclusively by light scattered by the nanoparticle. The corresponding Hamiltonian results from the coherent interference between the electric fields of the

tweezer and cavity respectively  $\hat{H} = -\frac{\alpha}{2}|\hat{\mathbf{E}}_{\text{cav}} + \hat{\mathbf{E}}_{\text{tw}}|^2$ , where  $\alpha$  is the polarizability of the nanosphere. The interference term  $\propto (\hat{\mathbf{E}}_{\text{cav}}^\dagger \hat{\mathbf{E}}_{\text{tw}} + \hat{\mathbf{E}}_{\text{cav}} \hat{\mathbf{E}}_{\text{tw}}^\dagger)$  gives rise to an effective CS potential:

$$\hat{V}_{\text{CS}}/\hbar = -E_d \cos(\phi + k\hat{Y}_c) e^{-(\hat{x}^2/w_x^2 + \hat{y}^2/w_y^2)} [\hat{a} + \hat{a}^\dagger]. \quad (1)$$

In the above, we omitted the  $\hat{z}$  dependence. The CS dynamics decouples into a 2+1 dynamics with  $x - y$  motion close in frequency and prone to hybridise; and a (typically) off-resonant  $z$  motion that is largely decoupled. We note  $z$  motion can be strongly cooled using feedback cooling [14, 15] but, in most experimental implementations,  $z$  is anyway moderately cooled due to a small unavoidable tilt relative to the cavity  $z$  axis. This effect and the full  $z$  dynamics is fully taken into account in numerical simulations, however, for brevity, it is not included in the present discussion.

In Eq. 1,  $Y_c$  represents the cavity axis. Relating the cavity coordinates to the tweezer frame is a simple rotation of the coordinate frames  $[X_c \ Y_c]^T = R_z(\theta)[x \ y]$ , where  $R_z(\theta)$  is the 2D rotation matrix.  $\phi$  is the displacement of the trap from an antinode. The tweezer waists  $w_x \simeq 1.068\mu\text{m}$  and  $w_y \simeq 0.928\mu\text{m}$  in the present set-up.

Linearised equations of motion are obtained using Eq.1, operators are expanded about equilibrium values, thus the optical field operators  $\hat{a} \rightarrow \bar{a} + \hat{a}(t)$  are expanded about the mean field, where  $n_p = |\bar{a}|^2$  is the mean photon occupancy of the cavity. This linearisation yields also optomechanical coupling terms  $g_x \hat{x}(\hat{a} + \hat{a}^\dagger)$  and  $g_y \hat{y}(\hat{a} + \hat{a}^\dagger)$ . In [23, 24] it was shown further that the CS potential also yields direct coupling terms  $g_{xy} \hat{x} \hat{y}$  of similar order to the usual linearised terms (thus do not vanish as the quantum occupancies are approached).

A study of hybridisation [23, 24] yielded solutions of the form  $\hat{x} \simeq \hat{x}(\omega) + \mathcal{R}_{xy}(\omega)\hat{y}(\omega)$  and  $\hat{y}(\omega) \simeq \hat{y}(\omega) + \mathcal{R}_{yx}(\omega)\hat{x}(\omega)$ , where  $\mathcal{R}_{xy}, \mathcal{R}_{yx}$  are hybridisation functions that are small in the weak coupling regime. In that case if  $\mathcal{R}_{xy} \simeq -\mathcal{R}_{yx}$  the above linear  $x - y$  hybridisation relation is already suggestive of a simple frame rotation.

One can show (see Appendix for details) that the resulting mechanical correlation spectra:

$$S_{xy}(\omega) \approx \text{Re}(\mathcal{R}_{yx}(\omega))S_{xx}(\omega) + \text{Re}(\mathcal{R}_{xy}(\omega))S_{yy}(\omega) \quad (2)$$

depend the real parts of the hybridisation function.  $\mathcal{R}_{xy} = -\mathcal{R}_{yx} = G_{xy}/(\omega_y - \omega_x)$  where  $G_{xy} = [i\eta_c(\omega)g_x g_y + g_{xy}]$  and  $\eta_c = \chi(\omega) - \chi^*(-\omega)$ ,  $\chi(\omega) = 1/(-i(\omega - \Delta) + \kappa/2)$  is the cavity susceptibility function. Hence we can write:

$$S_{xy}(\omega) = \Phi [S_{xx}(\omega) - S_{yy}(\omega)] \quad (3)$$

The above expression is generic to a 2D optomechanical system with non-zero  $g_x, g_y, g_{xy}$  in many typical regimes (it is assumed mechanical damping is  $\ll |\omega_y - \omega_x|$ ). However, the CS version has additional and unexpected features. The angle  $\Phi = \Phi_{\text{dyn}} + \Phi_{\text{CS}}$  can be

decomposed into two separate contributions (i) a cavity mediated term  $\Phi_{\text{dyn}} = \text{Re}(i\eta_c(\omega)g_x g_y)/(\omega_x - \omega_y)$  and (ii) a direct contribution  $\Phi_{\text{CS}} = g_{xy}/(\omega_x - \omega_y)$  arising from the static CS potential. It was found in [23] that the specific form of the couplings,  $g_x \simeq E_d k \sin \theta \sin \phi X_{zpf}$ ,  $g_y \simeq E_d k \cos \theta \sin \phi Y_{zpf}$  and

$$g_{xy} \simeq -g_x g_y 2\Delta \cot^2 \phi / (\kappa^2/4 + \Delta^2) \quad (4)$$

thus the combined dynamical and CS rotation becomes:

$$\Phi = \Phi_{\text{dyn}} + \Phi_{\text{CS}} = \frac{g_x g_y}{(\omega_y - \omega_x)} \left[ \text{Re}(i\eta_c) - \frac{2\Delta \cot^2 \phi}{(\kappa^2/4 + \Delta^2)} \right]. \quad (5)$$

The second term is positive since  $\Delta < 0$ , while rotate the modes in opposing directions.  $X_{zpf} = \sqrt{\hbar/(2m\omega_x)}$ ,  $Y_{zpf} = \sqrt{\hbar/(2m\omega_y)}$ .

The experimental PSDs  $S_{xx}, S_{yy}$  and correlation spectra at different trap positions are acquired at a constant pressure of  $3 \times 10^{-3}$  mbar with each time trace covering an observation time of 10 s. From these we obtain  $\Phi$  as a function of the trapping positions  $\phi$ .

The measured rotation in the mode orientations are shown in **Fig.2(a)** for two separate detunings which represent the two interesting limit cases. To model the experiments, for all results, we simulated nanospheres of radius  $R = 60.1\text{ nm}$ ; input power to the tweezer,  $P_{\text{tw}} = 0.485\text{ W}$ ;  $\theta \approx \pi/4$  (Fig.2 simulations (simulations makes me think of numerical integration but this analytical calculations right? ) employed  $\theta = 0.233\pi$ ).

*Behavior of the mechanical frequencies:* An interesting and unexpected observation is that the behavior of the frequencies mirrors the mode rotations: at the  $\phi \simeq \phi_c$ , they return to their unperturbed values. This is shown in **Fig.2(b)**, for two values of the optical detuning. Here, the experimental values are obtained by fitting the PSDs.

The unperturbed mechanical frequencies of this levitated optomechanical system are set by the tweezer trap:

$$(\omega_{(0)}^{(x,y)})^2 = \frac{\alpha \epsilon_{\text{tw}}^2}{m w_{x,y}^2} \quad (6)$$

where  $\epsilon_{\text{tw}}^2 = 4P_{\text{tw}}/(w_x w_y \pi c \epsilon_0)$  is related to the input power from the tweezer. In the presence of the cavity the coupling to the optical mode dynamics introduces an optical spring ‘softening’ (for red-detuned light) that is generic to all cavity optomechanical set-ups. In strong coupling regimes this can be a very large shift. Neglecting a correction for 2D  $x - y$  coupling [23, 24], the optical spring shift  $(\delta\omega_{\text{OS}}^{(j)})^2 = \text{Re}(-i2g_j^2 \omega_j^{(0)} \eta_c)$  with  $j = x, y$ .

However, for the coherent scattering set-up, there is a countervailing potential, obtained by linearising Eq.1, that ‘stiffens’ the mechanical frequencies. It is a static contribution, dependent on the mean photon occupancy

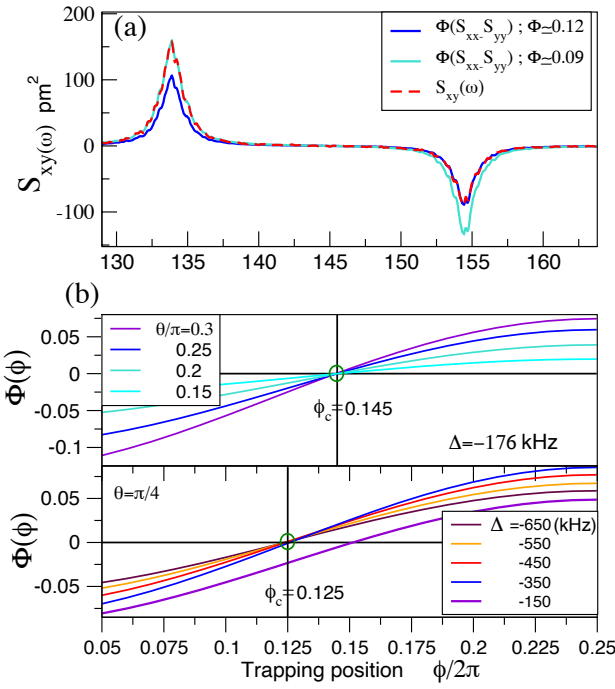


FIG. 3. (a) To measure mode rotation, we compare cross correlation spectra  $S_{xy}(\omega)$  with the rescaled difference between PSDs  $S_{xy}(\omega) \simeq \Phi(\phi) [S_{xx}(\omega) - S_{yy}(\omega)]$  to extract  $\Phi(\phi)$ . Plots show experimental  $S_{xy}$  at a node,  $\Delta = -360$  kHz and rescaled, measured,  $S_{xx} - S_{yy}$ . The rescaling gives excellent agreement, but there is a bias  $\Phi_\beta \approx 0.03$  arising from an imperfection in the orientation of the D-mirror, of the order of  $2^\circ$ , for the  $x$  detector. This yields a systematic shift between the scaling of all points obtained from the  $x$  peak (cyan) and the  $y$  peak (dark blue). In Fig.2 all  $x$  (cyan) data points are shifted by a constant,  $\Phi(\phi) \rightarrow \Phi(\phi) - \Phi_\beta$ . Upper red curve shows  $x - y$  hybridisation mediated by the cavity mode. (b) Illustrates the ‘locking’ of the mode orientation at  $\phi = \phi_c$ . (i) (upper panel): for  $\Delta = -176$  kHz, nearing resonance at  $\omega_{x,y} \sim 150$  kHz,  $\phi_c/2\pi = 0.145$ . At this point, for arbitrary tweezer polarisation  $\theta$  or input power, the modes remain at the unperturbed orientations. (ii) (lower panel) for large detuning  $-\Delta > 350$  kHz the locking point is  $\phi_c/2\pi = 0.125$ . For lower detunings,  $\phi_c$  moves towards the node and at  $\Delta = -150$  kHz,  $\phi_c/2\pi = 0.15$ . It is possible to optimise to close to  $\phi_c/2\pi \simeq 0.2$ .

of the cavity, thus can be considered an effect of co-trapping by the CS field. It takes the form  $(\delta\omega_{CS}^{(j)})^2 \simeq (E_d k^2 \sin^2 \theta / m) 2\Delta \cos^2 \phi / (\kappa^2 / 4 + \Delta^2)$ .

Hence the corrected frequencies combine the two contributions:  $(\omega_j)^2 = (\omega_j^{(0)})^2 + (\delta\omega_{CS}^{(j)})^2 + (\delta\omega_{OS}^{(j)})^2$  and may be written:

$$(\omega_j)^2 \simeq (\omega_j^{(0)})^2 + 2g_j^2 \omega_j^{(0)} \left[ \text{Re}(i\eta_c) - \frac{2\Delta \cot^2 \phi}{(\kappa^2 / 4 + \Delta^2)} \right] \quad (7)$$

It is clear from a comparison with Eq.5 that the multiplicative terms in square brackets are equivalent; thus

if they cancel for the mode orientations, they cancel for the frequency contributions. A more refined analysis, with consideration of weaker corrections and higher order terms will show that the  $\phi = \phi_c$  point is not identical for the frequencies and orientations, but it is quite close.

In Fig.3(a), the procedure for measuring the mode angles  $\Phi$  as a function of  $\phi$  is illustrated. A small imperfection in the orientation of the D-mirror, of the order of  $2^\circ$ , for the detection of  $x$  introduces a nonvanishing cross correlation with  $y$  even in absence of the cavity interaction. This translates into a constant bias in the evaluation of  $\Phi$ , which can be easily removed.

*Behavior of  $\phi_c$ :* the position of the cancellation point is shown in Fig.3(b). Clearly, from Eq.5 and Eq.7, there is no dependence of  $\phi_c$  on the experimental polarisation or input power. The upper panel shows this behavior for  $\Delta = -176$  kHz. The rate of rotation of the mode orientation varies considerably, but the cancellation point remains fixed at  $\phi_c/(2\pi) = 0.145$ . The lower panel shows that for large detuning,  $\phi_c$  is independent of  $\Delta$ . As shown in [23], at large detuning,  $\text{Re}(i\eta_c) \rightarrow \frac{2\Delta}{(\kappa^2 / 4 + \Delta^2)}$  is real, we obtain  $1 - 2 \cot^2 \phi_c = 0$ , implying  $\phi_c/(2\pi) = 0.125$  for all  $\Delta$ . However, as the detuning tends to resonance  $-\Delta \sim \omega_j^{(0)}$ ,  $\phi_c$  moves towards the node. For this particular cavity,  $\phi_c \simeq 0.15$  at resonance; but for lower  $\kappa$  one can approach  $\phi_c/(2\pi) = 0.2$ .

*Conclusions* CS set-ups approaches have had a disruptive effect on levitated cavity optomechanics for two key reasons: (i) they offer optomechanical coupling strengths an order of magnitude larger relative to earlier dispersive approaches (ii) in addition, the possibility of trapping at a cavity node, not possible in dispersive set-ups, offers an elegant solution to the detrimental impact of technical noise, including classical laser frequency noise, because of the drastic reduction in the number of photons in the cavity. Hence most CS experiments trap at a cavity node.

However, we show here that trapping from the node offers an unexpected regime where the CS potential very precisely cancels optomechanical perturbations to the mechanical mode orientations and their frequencies. In particular there exists a sweet spot for the tweezer within the cavity standing wave where the tweezer trap potential in effect appears unperturbed, yet one still retains the strong optomechanical damping.

We have explored experimentally regimes nearer resonance where the cancellation point moves towards the node and future studies in the good cavity regime combining of technical improvements to the frequency noise, combined with operation close to (but not exactly at) the node will be able to maximise the potential of this regime. This has important potential consequences for sensing applications. For example, the directional sensitivity of levitated nanoparticles aids the search for dark matter candidates since rejection of background events can be enhanced by the knowledge of the direction of the incoming dark matter candidate [26–28]. The same process can impede the formation of bright/dark mode formation in the strong coupling regime allowing efficient

2D quantum cooling, provided the increase of laser frequency noise can be managed.

We have explored experimentally regimes nearer resonance where the cancellation point moves towards the node. Future studies in the good cavity regime will combine technical improvements to the frequency noise with operation close to (but not exactly at) the node and will

thus be able to maximise the potential of this regime.

The authors would like to acknowledge helpful discussions with J. Gosling and M. Toroš. The authors acknowledge funding from the Engineering and Physical Sciences Research Council (EPSRC) Grant No. EP/N031105/1. H.F. and J. I. acknowledge EPSRC studentship funding via grant number EP/L015242/1 (H.F.) and EP/R513143/1 (J. I.).

---

[1] James Millen, Tania S Monteiro, Robert Pettit, and A Nick Vamivakas. Optomechanics with levitated particles. *Reports on Progress in Physics*, 83(2):026401, 2020.

[2] Oriol Romero-Isart, Mathieu L Juan, Romain Quidant, and J Ignacio Cirac. Toward quantum superposition of living organisms. *New Journal of Physics*, 12(3):033015, 2010.

[3] PF Barker and MN Shneider. Cavity cooling of an optically trapped nanoparticle. *Physical Review A*, 81(2):023826, 2010.

[4] Darrick E Chang, CA Regal, SB Papp, DJ Wilson, J Ye, O Painter, H Jeff Kimble, and P Zoller. Cavity opto-mechanics using an optically levitated nanosphere. *Proceedings of the National Academy of Sciences*, 107(3):1005–1010, 2010.

[5] GAT Pender, PF Barker, Florian Marquardt, James Millen, and TS Monteiro. Optomechanical cooling of levitated spheres with doubly resonant fields. *Physical Review A*, 85(2):021802, 2012.

[6] TS Monteiro, J Millen, GAT Pender, Florian Marquardt, D Chang, and PF Barker. Dynamics of levitated nanospheres: towards the strong coupling regime. *New Journal of Physics*, 15(1):015001, 2013.

[7] U Delić, M Reisenbauer, K Dare, D Grass, V Vuletić, N Kiesel, and M Aspelmeyer. Cooling of a levitated nanoparticle to the motional quantum ground state. *Science*, 367(6480):892–895, 2020.

[8] Nikolai Kiesel, Florian Blaser, Uroš Delić, David Grass, Rainer Kaltenbaek, and Markus Aspelmeyer. Cavity cooling of an optically levitated submicron particle. *Proceedings of the National Academy of Sciences*, 110(35):14180–14185, 2013.

[9] Peter Asenbaum, Stefan Kuhn, Stefan Nimmrichter, Uğur Sezer, and Markus Arndt. Cavity cooling of free silicon nanoparticles in high vacuum. *Nature communications*, 4(1):1–7, 2013.

[10] Pau Mestres, Johann Berthelot, Marko Spasenović, Jan Gieseler, Lukas Novotny, and Romain Quidant. Cooling and manipulation of a levitated nanoparticle with an optical fiber trap. *Applied Physics Letters*, 107(15):151102, 2015.

[11] J Millen, PZG Fonseca, T Mavrogordatos, TS Monteiro, and PF Barker. Cavity cooling a single charged levitated nanosphere. *Physical review letters*, 114(12):123602, 2015.

[12] PZG Fonseca, EB Aranas, J Millen, TS Monteiro, and PF Barker. Nonlinear dynamics and strong cavity cooling of levitated nanoparticles. *Physical review letters*, 117(17):173602, 2016.

[13] Lorenzo Magrini, Richard A Norte, Ralf Riedinger, Igor Marinković, David Grass, Uroš Delić, Simon Gröblacher, Sungkun Hong, and Markus Aspelmeyer. Near-field coupling of a levitated nanoparticle to a photonic crystal cavity. *Optica*, 5(12):1597–1602, 2018.

[14] Lorenzo Magrini, Philipp Rosenzweig, Constanze Bach, Andreas Deutschmann-Olek, Sebastian G Hofer, Sungkun Hong, Nikolai Kiesel, Andreas Kugi, and Markus Aspelmeyer. Optimal quantum control of mechanical motion at room temperature: ground-state cooling. *Nature*, 595:373–377, 2021.

[15] Felix Tebbenjohanns, Luisa Mattana, Massimiliano Rossi, Martin Frimmler, and Lukas Novotny. Quantum control of a nanoparticle optically levitated in cryogenic free space. *Nature*, 595:378–382, 2021.

[16] U Delić, M Reisenbauer, D Grass, N Kiesel, V Vuletić, and M Aspelmeyer. Cavity cooling of a levitated nanosphere by coherent scattering. *Physical review letters*, 122(12):123602, 2019.

[17] Dominik Windey, Carlos Gonzalez-Ballester, Patrick Maurer, Lukas Novotny, Oriol Romero-Isart, and René Reimann. Cavity-based 3d cooling of a levitated nanoparticle via coherent scattering. *Physical review letters*, 122(12):123601, 2019.

[18] Vladan Vuletić and Steven Chu. Laser cooling of atoms, ions, or molecules by coherent scattering. *Physical Review Letters*, 84(17):3787, 2000.

[19] Vladan Vuletić, Hilton W Chan, and Adam T Black. Three-dimensional cavity doppler cooling and cavity sideband cooling by coherent scattering. *Physical Review A*, 64(3):033405, 2001.

[20] Peter Domokos and Helmut Ritsch. Collective cooling and self-organization of atoms in a cavity. *Physical review letters*, 89(25):253003, 2002.

[21] David R Leibrandt, Jaroslaw Labaziewicz, Vladan Vuletić, and Isaac L Chuang. Cavity sideband cooling of a single trapped ion. *Physical review letters*, 103(10):103001, 2009.

[22] Mahdi Hosseini, Yiheng Duan, Kristin M Beck, Yu-Ting Chen, and Vladan Vuletić. Cavity cooling of many atoms. *Physical review letters*, 118(18):183601, 2017.

[23] M Toroš and TS Monteiro. Quantum sensing and cooling in three-dimensional levitated cavity optomechanics. *Physical Review Research*, 2(2):023228, 2020.

[24] M Toroš and TS Monteiro. Coherent-scattering two-dimensional cooling in levitated cavity optomechanics. *Physical Review Research*, 3:023071, 2021.

[25] AB Shkarin, NE Flowers-Jacobs, SW Hoch, AD Kashkanova, C Deutsch, J Reichel, and JGE Harris. Optically mediated hybridization between two mechanical modes. *Physical review letters*, 112(1):013602, 2014.

[26] S. Ahlen, N. Afshordi, and J. B. R. Battat et al. The

case for a directional dark matter detector and the status of current experimental efforts. *International Journal of Modern Physics A*, 25(01):1–51, January 2010.

[27] F. Mayet, A.M. Green, J.B.R. Battat, J. Billard, N. Bozorgnia, G.B. Gelmini, P. Gondolo, B.J. Kavanagh, S.K. Lee, D. Loomba, J. Monroe, B. Morgan, C.A.J. O’Hare, A.H.G. Peter, N.S. Phan, and S.E. Vahsen. A review of the discovery reach of directional dark matter detection. *Physics Reports*, 627:1–49, April 2016.

[28] Fernando Monteiro, Gadi Afek, Daniel Carney, Gordan Krnjaic, Jiaxiang Wang, and David C. Moore. Search for composite dark matter with optically levitated sensors. *Phys. Rev. Lett.*, 125:181102, Oct 2020.

## APPENDIX

### I. MECHANICAL FREQUENCIES

The combined tweezer-cavity Hamiltonian takes the form:

$$\hat{H} = -\frac{\alpha}{2} |\hat{\mathbf{E}}_{\text{cav}} + \hat{\mathbf{E}}_{\text{tw}}|^2, \quad (8)$$

where  $\hat{\mathbf{E}}_{\text{cav}}$  ( $\hat{\mathbf{E}}_{\text{tw}}$ ) denotes the cavity (tweezer) field,  $\alpha = 3\epsilon_0 V_s \frac{\epsilon_R - 1}{\epsilon_R + 2}$  is the polarizability of the nanosphere,  $V_s$  is the volume of the nanosphere,  $\epsilon_0$  is the permittivity of free space, and  $\epsilon_R$  is the relative dielectric permittivity.

We assume a coherent Gaussian tweezer field and replace the modes with c-numbers to find:

$$\hat{\mathbf{E}}_{\text{tw}} = \frac{\epsilon_{tw}}{2} \frac{1}{\sqrt{1 + (\frac{z}{z_R})^2}} e^{-\frac{\hat{x}^2}{w_x^2}} e^{-\frac{\hat{y}^2}{w_y^2}} e^{ik\hat{z} + i\Phi(\hat{z})} e^{-i\omega_{\text{tw}} t} \mathbf{e}_y + \text{cc} \quad (9)$$

where  $\Phi(z) = -\arctan \frac{z}{z_R}$  is the Gouy phase,  $z_R = \frac{\pi w_x w_y}{\lambda}$  is the Rayleigh range,  $w_x$  ( $w_y$ ) are the beam waist along the  $x$  ( $y$ ) axis,  $\epsilon_{tw} = \sqrt{\frac{4P_{\text{tw}}}{w_x w_y \pi \epsilon_0 c}}$  is the amplitude of the electric field,  $c$  is the speed of light,  $P_{\text{tw}}$  is the laser power,  $\omega_{\text{tw}}$  is the tweezer angular frequency,  $t$  is the time, and  $\hat{\mathbf{r}} = (\hat{x}, \hat{y}, \hat{z})$  is the position of the nanoparticle.  $\mathbf{e}_j$  are the unit vectors:  $\mathbf{e}_z$  is aligned with the symmetry axis of the tweezer field and  $\mathbf{e}_y$  is aligned with the polarization of the tweezer field.

The cavity field is given by:

$$\hat{\mathbf{E}}_{\text{cav}} = \epsilon_c \cos(k(Y_0^{(c)} + \hat{Y}^{(c)})) \mathbf{e}_y^c [\hat{a} + \hat{a}^\dagger], \quad (10)$$

where  $\epsilon_c = \sqrt{\frac{\hbar\omega_c}{2\epsilon_0 V_c}}$  is the amplitude at the center of the cavity,  $V_c$  is the cavity volume,  $\omega_c$  is the cavity frequency,  $\hat{a}$  ( $\hat{a}^\dagger$ ) is the annihilation (creation) operator,  $Y_0^{(c)}$  is an offset of the cavity coordinate system (centered at a cavity antinode) with respect to the tweezer coordinate system: hence  $\phi = kY_0^{(c)}$ .

The cavity  $X_c$ - $Y_c$  plane is rotated by an angle  $\theta$  with respect to the tweezer  $x$ - $y$  plane.

Note that for  $\theta = 0$  the tweezer polarization ( $y$ -axis) becomes aligned with the cavity symmetry axis ( $Y_c$ -axis). In particular, we have  $\hat{Y}^{(c)} = \sin(\theta)\hat{x} + \cos(\theta)\hat{y}$ .

We expand the Hamiltonian in Eq. (8) exploiting Eqs. (9) and (10) to obtain three terms:

$$\hat{H} = -\frac{\alpha}{2} |\hat{\mathbf{E}}_{\text{tw}}|^2 - \frac{\alpha}{2} |\hat{\mathbf{E}}_{\text{cav}}|^2 - \frac{\alpha \sin(\theta)}{2} (\hat{\mathbf{E}}_{\text{cav}}^\dagger \hat{\mathbf{E}}_{\text{tw}} + \hat{\mathbf{E}}_{\text{cav}} \hat{\mathbf{E}}_{\text{tw}}^\dagger), \quad (11)$$

where the terms on the right hand-side are the tweezer term, the cavity term, and the tweezer-cavity interaction term (from left to right). The first (tweezer field) term

dominates the trapping and primarily sets the three mechanical frequencies  $\omega_x$ ,  $\omega_y$ , and  $\omega_z$ .

The second term is the cavity intensity trapping: in earlier experiments with no tweezer trap and with cavities with very high photon occupancies  $n_p \gtrsim 10^{10}$  is provided the trapping and determined the mechanical frequencies. In CS setups it provides a negligible correction to the frequencies but is included in the numerics for numerical precision.

The third term, which we will denote as  $\hat{V}_{\text{int}}$ , is the most interesting and novel form of optomechanical interaction. This is the coherent scattering potential:

$$\frac{\hat{V}_{\text{CS}}}{\hbar} = -E_d \cos(\phi + k(\hat{x} \sin \theta + \hat{y} \cos \theta)) e^{-\frac{\hat{x}^2}{w_x^2}} e^{-\frac{\hat{y}^2}{w_y^2}} \hat{A};$$

where  $\hat{A} = [\hat{a} e^{-i(k\hat{z} + \Phi(\hat{z}))} + \hat{a}^\dagger e^{+i(k\hat{z} + \Phi(\hat{z}))}]$  (12)

$$\text{and } E_d = \frac{\alpha \epsilon_c \epsilon_{tw} \sin \theta}{2\hbar}. \quad (13)$$

while  $\phi = kY_0^{(c)}$  represents the effect of the shift between the origin of the cavity and tweezer. Linearising the above potential leads to the trap frequencies.

### A. tweezer trap frequencies

The mechanical  $x, y$  frequencies are set mainly by the tweezer trap  $-\frac{\alpha}{2}|\hat{\mathbf{E}}_{\text{tw}}|^2$ . Linearising leads to

$$(\omega_{tw}^{(x,y)})^2 = \frac{\alpha \epsilon_{tw}^2}{m w_{x,y}^2} \quad (14)$$

### B. co-trapping

This zero-th order frequency must be corrected by co-trapping by the coherent scattering potential in Eq.(1). This stiffens the zeroth order by a term obtained by linearisation. For the  $x, y$  frequencies this term depends on the mean cavity field:

$$\bar{\alpha} = \alpha_r + i\alpha_I = \frac{iE_d}{i\Delta + \kappa/2} \quad (15)$$

so  $\alpha_R = \frac{\Delta E_d \cos \phi}{\kappa^2/4 + \Delta^2}$ .

$$(\delta\omega_x)^2 \simeq -\frac{E_d \hbar}{m} 2\alpha_R \cos \phi [k^2 \sin^2 \theta + \frac{2}{w_x^2}]$$

$$(\delta\omega_y)^2 \simeq -\frac{E_d \hbar}{m} 2\alpha_R \cos \phi [k^2 \cos^2 \theta + \frac{2}{w_y^2}] \quad (16)$$

We note that the second term in the square brackets is small so  $(\delta\omega_x)^2 \simeq -\frac{E_d \hbar}{m} 2\alpha_R \cos \phi k^2 \sin^2 \theta$ . We see that as these corrections depend on  $\cos \phi$  they are zero at the node where  $\phi = \pi/2$  but increase to a maximum at the antinode.

### C. optical spring

For strong light-matter coupling  $g_{x,y}$ , an important perturbation is the optical spring shift that arises from the dynamics. If we write the usual "self energy" as  $\Sigma(\omega \simeq \omega_j) = -i2g_j^2 \eta(\omega \simeq \omega_j)$ , with  $j \equiv x, y$ , its imaginary part is the optical damping, while its *real* part represents the optical spring shifts:

$$(\delta\omega_{(OS,x)})^2 \simeq \omega_x \Re\{i2g_x^2 \eta_c(\omega = \omega_x)\}$$

$$(\delta\omega_{(OS,y)})^2 \simeq \omega_y \Re\{i2g_y^2 \eta_c(\omega = \omega_y)\} \quad (17)$$

(In [23], an additional correction was found, resulting from the intrinsic 2D dynamics, that here is negligible.) The optical spring shift depends on the dynamics, and the fluctuations in the optical mode. For red detuning, it softens the mechanical frequencies. It is strongest at the node and tends to zero as you approach the antinode since:

$$g_x \simeq E_d k \sin \theta \sin \phi X_{zpf}$$

$$g_y \simeq E_d k \cos \theta \sin \phi Y_{zpf} \quad (18)$$

$X_{zpf} = \sqrt{\hbar/(2m\omega_x)}$ ,  $Y_{zpf} = \sqrt{\hbar/(2m\omega_y)}$ . In addition, for the CS set up, there are also direct couplings  $g_{xy} \simeq -g_x g_y \frac{2\text{Re}(\bar{\alpha}) \cos \phi}{E_d \sin^2 \phi}$  related to the mean photon occupancy in the cavity. They are negligible at the nodes, but become stronger as  $\phi \rightarrow 0$ .

## II. THE $S_{xy}$ SPECTRUM

We showed in 2020 that we can correct the 1D displacements of  $x$  to allow for hybridisation as follows:

$$\hat{x}^{3D}(\omega) = \hat{x}^{1D}(\omega) + \mathcal{R}_{xy}(\omega) \hat{y}^{3D}(\omega) + \mathcal{G}_{xz}(\omega) \hat{z}^{3D}(\omega) \quad (19)$$

using the hybridisation function  $\mathcal{R}_{jk}(\omega)$  we introduced.

Neglecting the  $z$  motion, we have:

$$\hat{x}^{3D}(\omega) \simeq \hat{x}^{1D}(\omega) + \mathcal{R}_{xy}(\omega) \hat{y}^{3D}(\omega) \quad (20)$$

$$\hat{y}^{3D}(\omega) \simeq \hat{y}^{1D}(\omega) + \mathcal{R}_{yx}(\omega) \hat{x}^{3D}(\omega). \quad (21)$$

The terms  $\hat{x}^{1D}(\omega)$  and  $\hat{y}^{1D}(\omega)$  denote the optical and mechanical noises which would be present already in a one-dimensional analysis, so solutions with no hybridisation.

To obtain correlation spectra, we approximate

$$\hat{x}^{3D}(\omega) \simeq \hat{x}^{1D}(\omega) + \mathcal{R}_{xy}(\omega) \hat{y}^{1D}(\omega) \quad (22)$$

$$\hat{y}^{3D}(\omega) \simeq \hat{y}^{1D}(\omega) + \mathcal{R}_{yx}(\omega) \hat{x}^{1D}(\omega). \quad (23)$$

We drop the 3D superscript and assume that  $\hat{x}, \hat{y}$  are the exact solutions. We want the symmetrised PSD:

$$S_{xy}(\omega) = \frac{1}{2} \langle [\hat{x}]^\dagger \hat{y} + \langle [\hat{y}]^\dagger \hat{x} \rangle \rangle \quad (24)$$

But we know that the 1D components have negligible cross correlations  $S_{xy}^{1D} \simeq 0$ . so we can approximate

$$S_{xy}(\omega) \approx (\text{Re}(\mathcal{R}_{yx}(\omega))S_{xx}(\omega) + \text{Re}(\mathcal{R}_{xy}(\omega))S_{yy}(\omega)) \quad (25)$$

showing the cross-correlations are closely related to the real part of the hybridisation functions. We can readily show that the  $x - y$  modes are always anti-correlated (an experimental observation). by showing that the hybridisation functions  $\text{Re}\mathcal{R}_{xy} \approx -\text{Re}\mathcal{R}_{yx}$ . Starting from:

$$\mathcal{R}_{xy}(\omega) = \frac{i\mu_x(\omega)}{M_x(\omega)} [i\eta_c(\omega)g_xg_y + g_{xy}] \quad (26)$$

and:

$$\mathcal{R}_{yx}(\omega) = \frac{i\mu_y(\omega)}{M_y(\omega)} [i\eta_c(\omega)g_xg_y + g_{xy}] \quad (27)$$

The prefactor, where  $M_j(\omega) = 1 + g_j^2\mu_j(\omega)\eta_0(\omega)$  is peaked around one of the mechanical frequencies, i.e.  $\omega \approx \pm\omega_j$ . The  $\mu_j(\omega)$  are mechanical susceptibilities, while  $\eta_c$  is the optical susceptibility. The terms in the square brackets describe the interference between a direct,  $\propto g_{xy}$ , and a cavity mediated, indirect coupling,  $\propto g_xg_y$ , between any two displacements.

**Optical and mechanical susceptibilities** We have the usual mechanical susceptibility  $\mu_j(\omega) = \chi(\omega, \omega_j) - \chi^*(-\omega, \omega_j)$  and optical susceptibility  $\eta_0(\omega) = \chi(\omega, -\Delta) - \chi^*(-\omega, -\Delta)$ , where eg  $\chi(\omega, \omega_x) = [-i(\omega - \omega_x) + \frac{\Gamma}{2}]^{-1}$  and  $\chi(\omega, \Delta) = [-i(\omega - \Delta) + \frac{\kappa}{2}]^{-1}$

### A. anticorrelation

However the observed anticorrelation arises from the prefactor  $\frac{i\mu_j(\omega)}{M_j(\omega)}$  in Eq.27. ie

$$\mathcal{R}_{xy}(\omega) = G_{yx} \frac{i\mu_x(\omega)}{M_x(\omega)} \quad (28)$$

$$\mathcal{R}_{yx}(\omega) = G_{xy} \frac{i\mu_y(\omega)}{M_y(\omega)}. \quad (29)$$

$G_{xy} = G_{yx} = [i\eta_c(\omega)g_xg_y + g_{xy}]$  So the  $G_{xy}$  is formally the same in both cases. However we are interested in  $\mathcal{R}_{xy}(\omega \simeq \omega_y)$  and  $\mathcal{R}_{yx}(\omega \simeq \omega_x)$ .

$$\mu_x(\omega = \omega_y) \simeq [-i(\omega_y - \omega_x) + \frac{\Gamma}{2}]^{-1} \simeq i/(\omega_y - \omega_x) \quad (30)$$

and

$$\mu_y(\omega = \omega_x) \simeq [-i(\omega_x - \omega_y) + \frac{\Gamma}{2}]^{-1} \simeq i/(\omega_x - \omega_y) \quad (31)$$

Since  $\kappa \gg |\omega_x - \omega_y|$  the cavity susceptibility function  $\eta_c(\omega)$  is insensitive so  $G_{xy}(\omega_y) \simeq G_{yx}(\omega_x)$ .

However it is the denominator in Eq.29 that implies that  $\mathcal{R}_{xy} = -\mathcal{R}_{yx}$  and thus that  $S_{xy}$  spectra indicate the  $x - y$  motions are always anti-correlated.

Returning to our approximate PSD:

$$S_{xy}(\omega) \approx G_{xy} \left( \Im \left[ \frac{\mu_y(\omega_x)}{M_y(\omega_x)} \right] S_{xx} + \Im \left[ \frac{\mu_x(\omega_y)}{M_x(\omega)_y} \right] S_{yy} \right) \quad (32)$$

Finally, we can make a further approximation (we can justify it) that  $\Im \left[ \frac{\mu_y(\omega_x)}{M_y(\omega_x)} \right] \approx 1/(\omega_y - \omega_x)$  and the converse. So we can approximate:

$$S_{xy}(\omega) \approx \frac{G_{xy}(\omega)}{\omega_x - \omega_y} [S_{xx}(\omega) - S_{yy}(\omega)] \quad (33)$$

In the figure we test this simple expression against the exact QLT anticorrelation spectrum. We use  $G_{xy} = [i\eta_c(\omega)g_xg_y + g_{xy}]$  in the figure for more accuracy but for insight, Eq.12 is useful too. We can see that there is remarkable agreement everywhere.

So the anti correlation arises because the susceptibility for  $y$  involves upconverting in energy whereas  $x$  downconverts. The opposite sign is generic. The overall sign flips when  $G_{xy}$  changes sign. We can see that for  $\theta = 3/4\pi$  then  $g_x = -g_y$  so there is a global sign flip.

### B. Suppression of hybridisation at large detuning

The term in square brackets in Eq.27, ie  $G_{xy} = G_{yx} = [i\eta_c(\omega)g_xg_y + g_{xy}]$  suppresses hybridisation in between node and antinode. Since the direct coupling  $g_{xy} \simeq -g_xg_y \frac{2\text{Re}(\bar{\alpha})\cos\phi}{E_d \sin^2\phi}$ , and  $\bar{\alpha} \simeq iE_d \cos(\phi)[\Delta + i\kappa/2]^{-1}$ :

$$g_{xy} \simeq g_xg_y \left[ \frac{2\Delta \cot^2\phi}{\Delta^2 + \frac{\kappa^2}{4}} \right]. \quad (34)$$

Thus depending on the positioning,  $\Delta$  or  $\kappa$ , the direct couplings contribution can be similar or exceed the cavity mediated coupling.

It was shown in [23] that for  $\Delta \gg \omega_j$ , at  $\phi = \pi/4$  the  $x - y$  hybridisation almost fully vanishes. Although both direct and indirect contributions are strong they interfere destructively. We can show that  $i\eta^{(0)}(\omega) \rightarrow \frac{-2\Delta}{(\kappa/2)^2 + \Delta^2}$  if  $-\Delta \gg \omega$  (and we are interested primarily in the region  $\omega \sim \omega_j$ ). Thus for large  $-\Delta$ :

$$G_{xy}(\omega) \approx g_xg_y \left[ \frac{-2\Delta}{\Delta^2 + (\kappa/2)^2} \right] [1 - \cot^2\phi], \quad (35)$$

and the  $x, y$  coupling  $G_{xy}^{3D}(\omega)$  thus vanishes.

In the present experimental study we are not necessarily in the large detuning limit so we consider other regimes including  $-\Delta \sim \omega_{x,y}$  and find the cancellation  $\phi = \phi_c$  moves towards the node.

### III. EXPERIMENTAL MEASUREMENT OF $\phi_c$

The interesting thing about the experiment is that it shows the substantial shift in the cancellation point to  $\phi_c/2\pi = 0.15 - 0.2$  which is closer to the node at  $\phi_c/2\pi = 0.25$  than the  $\phi_c/2\pi = 0.125$  predicted by Eq.35 that is valid for large detuning. This might be helpful as the cancellation point suppresses the dark mode that forms when the cavity mediated term is dominant (and for sideband resolved, it is a strong coupling effect). The

closer to the node, the lower the cavity photon occupancy so that is desirable.

We now define a mode rotation angle  $\Phi = 1/2[\text{Re}[R_{xy}] - \text{Re}[R_{yx}]]$ , or  $\frac{G_{xy}(\omega)}{\omega_x - \omega_y}$  using the ratio of the PSDs that may be extracted experimentally:

$$S_{xy}(\omega) = \Phi(\phi) [S_{xx}(\omega) - S_{yy}(\omega)] \quad (36)$$